

Solution X-ray Absorption Fine Structure Study of the Eu^{2+} and Sr^{2+} Ions: Unexpected Solvent and Metal Ion Dependencies of the Solvation Numbers

Gilles Moreau,[†] Rosario Scopelliti,[†] Lothar Helm,[†] Juris Purans,^{†,‡} and André E. Merbach^{*,†}

Institute of Molecular and Biological Chemistry, Swiss Federal Institute of Technology Lausanne, EPFL-BCH, CH-1015 Lausanne, Switzerland, and Institute of Solid State Physics, Kengaraga str. 8, LV-1063 Riga, Latvia

Received: May 3, 2002; In Final Form: August 9, 2002

Structural parameters of the Sr^{2+} and, for the first time, of the Eu^{2+} ions in nonaqueous solutions were determined by the X-ray absorption fine structure (XAFS) method and compared with those of the aqua ions. For both Eu^{2+} and Sr^{2+} ions, a decrease in coordination number (N) and metal-to-solvent distances was found along the increasingly solvating $\text{MeCN} < \text{H}_2\text{O} \ll \text{DMF} < \text{DMSO}$ solvent series: for strontium, $N = 8$ with $[\text{Sr}(\text{MeCN})_8]^{2+}$ (2.665(6) Å) and $[\text{Sr}(\text{H}_2\text{O})_8]^{2+}$ (2.600(3) Å) and $N = 7$ with $[\text{Sr}(\text{DMF})_7]^{2+}$ (2.555(5) Å) and $[\text{Sr}(\text{DMSO})_7]^{2+}$ (2.540(7) Å); for europium(II), $N = 8$ with $[\text{Eu}(\text{MeCN})_8]^{2+}$ (2.640(4) Å), $N = 7$ with $[\text{Eu}(\text{H}_2\text{O})_7]^{2+}$ (2.584(5) Å), and $N = 6$ with $[\text{Eu}(\text{DMF})_6]^{2+}$ (2.541(3) Å) and by extrapolation $[\text{Eu}(\text{DMSO})_6]^{2+}$ (2.525 Å). Smaller coordination numbers are observed for the Eu^{2+} ion in O-coordinating solvents. The ionic radii of both Sr^{2+} and Eu^{2+} ions are very similar, but the slightly softer character of the Eu^{2+} ion leads to shorter M–N and longer M–O bonds.

Introduction

Solvation is one of the most important chemical properties of a metal ion in solution because the solvent exchange reaction is often used as a model for the interpretation of the substitution reaction mechanisms. As a prerequisite, it is important to know the structure of the solvated ion in solution to interpret and understand the thermodynamics and kinetics of the complex formation reactions. The relative strength of the metal ion–solvent interactions is dependent on the electron-pair donor and acceptor properties of both solvent and metal ion. To better understand the solvation process of an ion in solution, it is therefore necessary to study it in a series of solvents with different properties. Pursuing the parallel structural study of the Eu^{2+} and Sr^{2+} ions in aqueous medium,¹ we have investigated the solvation structure of these two ions in dimethyl formamide (DMF), dimethyl sulfoxide (DMSO), and acetonitrile (MeCN) solutions in the present work.

Whereas water is a hard polar and protic solvent with extensive hydrogen bonding, DMF and DMSO are aprotic solvents with high dipole moments and medium permittivities.² For these three solvents, the solvation of hard metal ions such as Sr^{2+} and presumably Eu^{2+} occurs via the solvent oxygen atom. MeCN is a softer nitrogen-binding solvent with dipole moment and permittivity similar to those of the DMF and DMSO.² Hard metal ions are readily dissolved by water, DMF, and DMSO and have a relatively low solubility in MeCN.

The available information on the properties of the Eu^{2+} ion is poor, especially in nonaqueous solutions, owing to its redox instability. It has been pointed out that strong similarities exist between divalent lanthanide ions and the alkaline earth metals.³ However, until now, quantitative assessment of the similarity of these groups of elements remains extremely limited.³

In the present work, the structures of the solvated Eu^{2+} and Sr^{2+} ions are studied in the oxygen-donor solvents dimethyl sulfoxide and *N,N*-dimethyl formamide and in the nitrogen-donor acetonitrile. The experimental L₃-edge X-ray absorption fine structure (XAFS) spectra of Eu^{2+} , as well as the Sr^{2+} K-edge, have been measured, analyzed, and compared using the cumulant approach combined with efficient analysis techniques.^{4–6} Both theoretical (calculated *ab initio*⁷) and experimental (extracted from crystalline reference⁸) phases and amplitudes have been used.

Experimental Section

Chemicals. $\text{Sr}(\text{DMF})_2(\text{O}_3\text{SCF}_3)_2$ and $\text{Sr}(\text{DMSO})_2(\text{O}_3\text{SCF}_3)_2$ were prepared under nitrogen according to the following procedure. Two equivalents of 98% $\text{CF}_3\text{SO}_3\text{H}$ (triflic acid) was added to a suspension of 1 g of SrCO_3 in 10 equiv of $\text{HC}(\text{OEt})_3$. After filtration, 2.2 equiv of the desired solvent was added, and the solution was evaporated gently under vacuum until precipitation. The precipitate was redissolved by heating, and crystals were filtered off by centrifugation after slow cooling. Anal. Calcd for $\text{Sr}(\text{DMF})_2(\text{O}_3\text{SCF}_3)_2$: C, 18.1; H, 2.6; N, 5.3; Sr, 16.5. Found: C, 18.1; H, 2.4; N, 5.0; Sr, 16.9. Anal. Calcd for $\text{Sr}(\text{DMSO})_2(\text{O}_3\text{SCF}_3)_2$: C, 13.3; H, 2.2; Sr, 16.2. Found: C, 13.6; H, 2.0; Sr, 17.0. The following procedure was used to obtain the starting materials used in the preparation of the Eu^{2+} and Sr^{2+} solutions. Two equivalents of 98% triflic acid was added to a suspension of 1 g of EuCO_3 ⁹ or SrCO_3 in 10 equiv of $\text{HC}(\text{OEt})_3$. After filtration, pentane was added to the solution to precipitate quantitatively the metal triflate. After filtration and 72 h under vacuum, $\text{Eu}(\text{O}_3\text{SCF}_3)_2 \cdot \text{EtOH}$ or $\text{Sr}(\text{O}_3\text{SCF}_3)_2 \cdot 1/2\text{EtOH}$ salts were obtained. Anal. Calcd for $\text{Eu}(\text{O}_3\text{SCF}_3)_2 \cdot \text{EtOH}$: C, 9.6; H, 1.2; Eu, 30.6. Found: C, 9.5; H, 1.1; Eu, 29.0. Anal. Calcd for $\text{Sr}(\text{O}_3\text{SCF}_3)_2 \cdot 1/2\text{EtOH}$: C, 8.8; H, 0.7; Sr, 21.4. Found: C, 8.8; H, 0.7; Sr, 22.0.

For all compounds, the absence of water was checked by Karl Fischer titration. Triflic acid (98%) was purchased from Aldrich Chemicals. All commercial compounds were used as

* To whom correspondence should be addressed. Phone: +41-21-693 98 71. Fax: +41-21-693 98 75. E-mail: andre.merbach@epfl.ch.

[†] Swiss Federal Institute of Technology Lausanne.

[‡] Institute of Solid State Physics.

TABLE 1: Crystal Data and Details of the Structure Determination

	Sr(DMF) ₂ (O ₃ SCF ₃) ₂	Sr(DMSO) ₂ (O ₃ SCF ₃) ₂
chemical formula	C ₈ H ₁₄ F ₆ N ₂ O ₈ S ₂ Sr	C ₆ H ₁₂ F ₆ O ₈ S ₄ Sr
fw	531.95	542.02
cryst syst	orthorhombic	monoclinic
space group	<i>Ibam</i>	<i>I2/a</i>
<i>a</i> (Å)	11.6800(10)	8.4221(13)
<i>b</i> (Å)	20.5299(18)	11.5766(16)
<i>c</i> (Å)	8.0429(15)	18.420(3)
β (deg)	90	93.263(12)
vol (Å ³)	1928.6(4)	1793.0(4)
<i>Z</i>	4	4
<i>D</i> _{calcd} (g cm ⁻³)	1.832	2.008
<i>F</i> (000)	1056	1072
μ (mm ⁻¹)	3.105	3.564
temp (K)	143	143
wavelength (Å)	0.710 73	0.710 73
measd reflns	5620	5084
unique reflns	874	1512
unique reflns [<i>I</i> > 2 σ (<i>I</i>)]	815	1165
data/params	874/93	1512/115
<i>R</i> ^a [<i>I</i> > 2 σ (<i>I</i>)]	0.0346	0.0919
wR2 ^a (all data)	0.0934	0.2626
GOF ^b	1.086	1.179

^a $R = \sum |F_o| - |F_c| / \sum |F_o|$; wR2 = $\{\sum [w(F_o^2 - F_c^2)^2] / \sum [w(F_o^2)^2]\}^{1/2}$.
^b GOF = $\{\sum [w(F_o^2 - F_c^2)^2] / (n - p)\}^{1/2}$, where *n* is the number of data and *p* is the number of parameters refined.

received. Solvents were freshly distilled before use according to the literature-recommended methods.² They were distilled under oxygen-free nitrogen, degassed by a triple freeze–pump–thaw cycle, and stored in an oxygen-free and water-free glovebox. The Karl Fischer coulometric titration gave for DMF, DMSO, and MeCN a respective maximum water amount of 18, 12, and 10 ppm.

Preparation of the Samples. The Sr²⁺ solutions (0.15 M in DMF, 0.15 M in DMSO, 0.09 M in MeCN) were prepared by dissolution of the Sr(O₃SCF₃)₂·1/2EtOH salt into pure solvent. The Eu²⁺ solutions (0.15 M in DMF, 0.10 M in MeCN) were prepared by dissolution of the Eu(O₃SCF₃)₂·EtOH salt into pure solvent. Additionally, the solutions were treated by amalgamated zinc just before the XAFS measurements to avoid traces of Eu³⁺.¹ Concentrations were checked by complexometric titration. The L₃-edge X-ray absorption near-edge structure (XANES) measurements have confirmed that sealed oxygen-free samples of ca. 0.1 M Eu(O₃SCF₃)₂ nonaqueous solutions are stable in the multipurpose cell that we used for at least 5 h (less than 0.2% Eu³⁺).¹

The reference crystalline samples Sr(DMF)₂(O₃SCF₃)₂ and Sr(DMSO)₂(O₃SCF₃)₂ were finely ground and mechanically mixed with cellulose powder to give pressed pellets with thickness chosen to obtain an absorption jump value of about 1.

All of the compounds and solutions were prepared, handled, and stored in the dry nitrogen atmosphere of a glovebox to avoid both oxidation of the Eu²⁺ and water contamination of the compounds and solutions.

X-ray Experimental Section. Suitable crystals of Sr(DMF)₂(O₃SCF₃)₂ and Sr(DMSO)₂(O₃SCF₃)₂ were obtained as described and mounted in glass capillaries. Crystal data and structure refinement details are listed in Table 1. Data collections were performed on an Oxford diffraction Kuma4 sapphire CCD and data reductions were carried out with CrysAlis RED.¹⁰ Absorption correction was applied to both data sets. For the Sr(DMF)₂(O₃SCF₃)₂, the MULTI–SCAN semiempirical method¹¹ has been employed, whereas for the Sr(DMSO)₂(O₃SCF₃)₂, the DIFABS empirical method¹² has been used. Structure solution

for both compounds was performed with SIR97.¹³ The structures were refined using the full-matrix least-squares on *F*² with all non-H atoms anisotropically defined. H atoms were placed in calculated positions using the “riding model” for Sr(DMSO)₂(O₃SCF₃)₂, whereas they have been treated as free isotropic atoms for Sr(DMF)₂(O₃SCF₃)₂ (in this latter case, likely because of disorder combined with special position for a methyl group, the distances C–H and H···H have been restrained to get a reasonable geometry). Space group determination, structure solution, refinement, molecular graphics, and geometrical calculation have been carried out on both structures with the SHELXTL software package.¹⁴

XAFS Measurements. XAFS measurements were performed at the LURE synchrotron radiation facility (Orsay, France) on the DCI D21 (XAS 2) beam line. Positron-beam energy and average current were 1.85 GeV and 320–250 mA, respectively. The XAFS spectra of the Eu L₃-edge (6976 eV; scan 6900–7650 eV) and Sr K-edge (16 105 eV; 16 000–17 000 eV) were measured in transmission mode. The synchrotron radiation was monochromatized using the Si(311) double-crystal monochromator, and in the case of the Eu L₃-edge, harmonic rejection was achieved using dedicated mirrors. The experimental spectra were measured using two ionization chambers (filled with air for Eu and with Ar for Sr measurements) with a count rate of 2 s per point, an energy resolution of 1 or 2 eV, a 0.5 or 1 eV step in the XANES region, and a 1 or 2 eV step in the extended x-ray absorption fine structure (EXAFS) region for the Eu L₃-edge and the Sr K-edge, respectively. A multipurpose X-ray absorption cell¹⁵ was used for the in-situ XAFS measurements of sealed oxygen- and water-free solutions. The measurements were done at an optical length of 1–1.5 mm for Eu and 4–8 mm for Sr, resulting in values of the absorption jump of about 0.5 (WL amplitude about 2) for Eu and about 1 for Sr. At least two complete and identical XAFS scans were collected for each solution. All samples were measured at room temperature (20–25 °C).

Data Analysis. The experimental XAFS data were treated using the EDA software package¹⁶ in a way similar to the one used in the study of the Eu²⁺ and Sr²⁺ aqua ions.¹ The obtained XAFS spectra, $\chi(E)$, were converted to the *k*-space of the photoelectron wavevector, defined as $k = \sqrt{(2m/\hbar^2)(E - E_0)}$, where (*E* – *E*₀) is the photoelectron kinetic energy measured. The experimental XAFS spectra $\chi(k)$ of both Eu and Sr were multiplied by a factor *k*³ to compensate for the decrease of amplitude with increasing wavevector value.

The experimental XAFS spectra (Figures 1 and 2) were Fourier-transformed (FT) with a Kaiser–Bessel window in the 0–12 Å⁻¹ range for Eu and 0–13 Å⁻¹ for Sr using a photoelectron phase-shift correction. The first shell XAFS contributions were singled out by back FT procedure in the 1.9–3.2 Å range for both Eu²⁺ and Sr²⁺. Use of the phase-shift correction allowed us to reduce the nonstructural peaks distorting the baseline and led to a significant sharpening of the first shell peak, allowing a more precise Fourier filtering.¹ The use of the corrected Fourier-filtering procedure led to a real increase in the fitting reproducibility when playing on the parameters.

The first-shell XAFS spectra were fitted using the single-scattering curved-wave formalism with cumulant expansion:⁴

$$\chi(k) = \frac{N}{kC_1} f(\pi, k) \exp\left(-\frac{2C_1}{\lambda(k)}\right) \exp\left(-2C_2k^2 + \frac{2}{3}C_4k^4\right) \times \sin\left(2kC_1 - \frac{4}{3}C_3k^3 + \phi(\pi, k)\right) \quad (1)$$

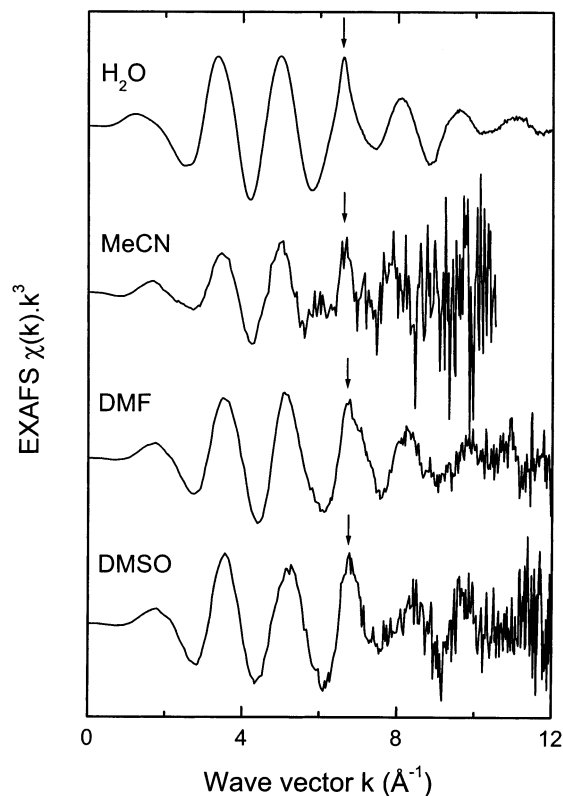


Figure 1. Experimental XAFS spectra of $\text{Sr}(\text{O}_3\text{SCF}_3)_2$ 0.14 M in H_2O , 0.09 M in MeCN, 0.15 M in DMF, and 0.15 M in DMSO (arrows, see text).

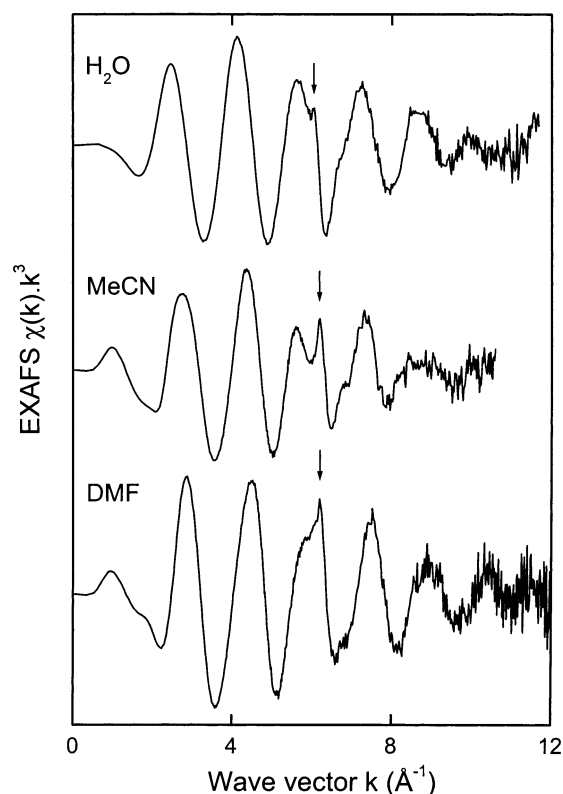


Figure 2. Experimental XAFS spectra of $\text{Eu}(\text{O}_3\text{SCF}_3)_2$ 0.15 M in H_2O , 0.10 M in MeCN, and 0.15 M in DMF (arrows, see text).

where N is the coordination number and $C_2 = \sigma^2$ is the Debye–Waller (DW) factor (in harmonic approximation). The higher-order cumulants C_3 and C_4 characterize the deviation of the distribution of distances from a Gaussian shape. The first

TABLE 2: Muffin-Tin Radii (R_{MT}) for the First-Shell Atoms^a

computed cluster	R_{MT} (Sr)	R_{MT} (O/N)	R_{MT} (Eu)	R_{MT} (O/N)
$\text{MO}_8(\text{H}_2\text{O})_{16}(\text{OH})_8$ ^b	1.491	1.143	1.481	1.126
$\text{M}(\text{OCNC}_2)_4(\text{O}_3\text{SCF}_3)_4$ ^c	1.658	0.730	1.662	0.732
$\text{M}(\text{OSC}_2)_6$ ^d	1.563	0.820	1.566	0.819
$\text{M}(\text{OSC}_2)_8$ ^e	1.634	0.758	1.637	0.758
$\text{M}(\text{NCC})_6$ ^f	1.724	0.634	1.726	0.636
$\text{M}(\text{NCC})_8$ ^g	1.666	0.689	1.668	0.690

^a All of the muffin-tin radii are given in Å. ^b Based on $[\text{Sr}(\text{H}_2\text{O})_8](\text{OH})_2$ XRD structure, ref 18 (scaling factor, SF = 1). ^c $\text{Sr}(\text{DMF})_2(\text{O}_3\text{SCF}_3)_2$, this study (SF = 1). ^d $[\text{Cd}(\text{DMSO})_6][\text{CdI}_4]$, ref 19 (SF = 1.1). ^e $[\text{Gd}(\text{DMSO})_8][\text{Fe}(\text{CN})_6]$, ref 20 (SF = 1.05). ^f $[\text{Na}(\text{MeCN})_6][\text{TaCl}_6]$, ref 21 (SF = 1.05). ^g $[\text{Yb}(\text{MeCN})_8](\text{AlCl}_4)_3$, ref 22 (SF = 1.1).

cumulant C_1 is closely related to the interatomic distance R .¹⁷ $\lambda(k) = k\Gamma$ is an adjustable function that models the low k damping factors. As in previous works,¹ the Γ parameter was allowed to vary during the fitting procedure for fine adjustment between theoretical calculations and experiment. This parameter also allows us to compensate for the FT boundary effects and was found within classical range (from 0 to 0.1).

Phases and Amplitudes. In this paper, the strontium XAFS data were analyzed using two different approaches: the phases $\phi(\pi, k)$ and amplitudes $f(\pi, k)$ were either calculated or obtained experimentally.

We showed in a precedent paper¹ the importance in the choice of the reference cluster used for the theoretical backscattering amplitudes and phases calculations using the FEFF6 code.⁷ To find a cluster that mimics well the possible environment of the Eu^{2+} and Sr^{2+} ions in solution, we checked the literature for crystallographic structures in which a cation is surrounded only by the solvent molecules, that is, DMF, DMSO, or MeCN. Because of their ionic radii close to the Eu^{2+} and Sr^{2+} ones, the following compounds have been retained: (1) $[\text{Sr}(\text{H}_2\text{O})_8](\text{OH})_2$,^{1,18} (2) $\text{Sr}(\text{DMF})_2(\text{O}_3\text{SCF}_3)_2$, (3) $[\text{Cd}(\text{DMSO})_6][\text{CdI}_4]$,¹⁹ (4) $[\text{Gd}(\text{DMSO})_8][\text{Fe}(\text{CN})_6]$,²⁰ (5) $[\text{Na}(\text{MeCN})_6][\text{TaCl}_6]$,²¹ and (6) $[\text{Yb}(\text{MeCN})_8](\text{AlCl}_4)_3$.²² The ionic radii of these ions being slightly different than those of the Eu^{2+} and Sr^{2+} , scaling factors were applied for the M–O or M–N distances to match the distances in the system studied (see Table 2 for detail). Using the respective crystallographic coordinates of the selected compounds, we calculated the following clusters to obtain theoretical $\phi(\pi, k)$ and $f(\pi, k)$ functions: (1) $\text{MO}_8(\text{H}_2\text{O})_{16}(\text{OH})_8$, (2) $\text{M}(\text{OCNC}_2)_4(\text{O}_3\text{SCF}_3)_4$, (3) $\text{M}(\text{OSC}_2)_6$, (4) $\text{M}(\text{OSC}_2)_8$, (5) $\text{M}(\text{NCC})_6$, and (6) $\text{M}(\text{NCC})_8$. The computed muffin-tin radii for the different clusters are detailed in Table 2.

Because the threshold energy of the photoelectron E_0 is defined in the FEFF6 code⁷ relative to the Fermi level and depends on the muffin-tin radii, the spectra have to be corrected to avoid E_0 difference errors in the fitting process. Consequently, the phase differences between theoretical and experimental spectra were set to zero at low k , according to Bunker and Stern's criterion,²³ and E_0 was allowed to vary for fine adjustment during the fitting procedure.

Experimental $f(\pi, k)$ and $\phi(\pi, k)$ were extracted from the experimental XAFS data obtained on the crystalline $\text{Sr}(\text{DMF})_2(\text{O}_3\text{SCF}_3)_2$. These functions were obtained assuming Gaussian distribution of distances with $N = 8$ and $R = 2.585$ Å, from the crystallographic data, and $\sigma^2 = 0.0106$ Å² from the fit with theoretical phase and amplitude. Experimental $f(\pi, k)$ and $\phi(\pi, k)$ were also extracted from the experimental XAFS spectra of the Eu^{2+} and Sr^{2+} aqueous solution and normalized according to the structural parameters determined in ref 1.

Note that use of experimental phases and amplitudes allows, to a certain extent, the compensation of systematic errors

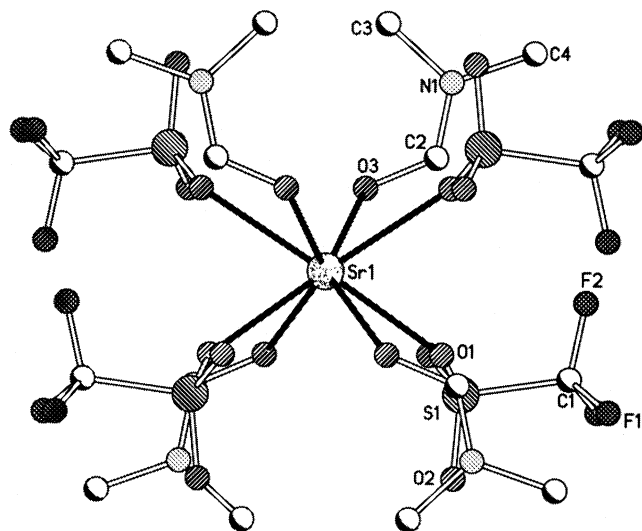


Figure 3. Ball-and-stick representation of the $\text{Sr}(\text{DMF})_2(\text{O}_3\text{SCF}_3)_2$ coordination polyhedron.

because they include the contribution of the mean free path, of the multielectron amplitude reduction factor S_0^2 , of glitches and of resolution, reducing the number of adjustable parameters and consequently increasing the reliability of the fitted results. To ensure the phases and amplitudes transferability and to allow estimation of systematic errors, all of the data were analyzed in a similar way, using the same theoretical phases and amplitudes, filtering procedures, and parameters.

Multielectron Transition Effect. The same kind of anomalous features observed in the Sr^{2+} aqua ion XAFS spectrum^{1,18,24} are present in the XAFS spectra of the Sr^{2+} ion in the DMF, DMSO, and MeCN solutions (Figure 1). This anomalous feature due to the simultaneous excitation of $1s3d$ electrons is indicated by an arrow in Figure 1 and arises around 6.4 \AA^{-1} . Similar

multielectron transition effects (MET) features are found for the Eu^{2+} solutions at ca. 6.2 \AA^{-1} (Figure 2). As in the case of the Eu^{2+} aqua ion,¹ we attribute this sharp contribution to a $2p4d$ double-electron transition.

As we already stated,¹ these anomalies result after Fourier transform in humps distorting the base of the major peak standing for the first-shell Sr–O or Eu–O peak, especially at low distances. But the use of the new 2001 version of the EDA software package¹⁶ combined with the phase-shift corrected Fourier filtration allowed us a greater precision in the zero-line removal and in the Fourier-filtering processes, so no subsequent additional MET removal was necessary.

Results

X-ray Crystal Structure of $\text{Sr}(\text{DMF})_2(\text{O}_3\text{SCF}_3)_2$ and $\text{Sr}(\text{DMSO})_2(\text{O}_3\text{SCF}_3)_2$. The crystal structure of $\text{Sr}(\text{DMF})_2(\text{O}_3\text{SCF}_3)_2$ (Figure 3) consists of eight coordinate Sr^{2+} cations lying on a 222 symmetry site. Each metal ion is linked to four DMF ligands and to four CF_3SO_3^- . Each ligand lies on a symmetry plane and bridges two Sr^{2+} ions by means of one oxygen atom in the case of the DMF and by means of two different oxygen atoms in the case of CF_3SO_3^- . Thus, the overall structure (Figure 4) is formed by infinite one-dimensional chains along the c axis. The eight oxygen atoms around each Sr^{2+} ion form an almost perfect square antiprism geometry (with a characteristic α angle²⁵ of 57.5° for O1 and 57.7° for O3). Sr–O bond distances reflect the different nature of the two ligands [Sr1–O1, $2.567(2) \text{ \AA}$; Sr1–O3, $2.578(2) \text{ \AA}$], leading to an average Sr–O bond length of 2.572 \AA . Within the polymeric chains responsible for the crystal packing, the Sr \cdots Sr distance is $4.021(1) \text{ \AA}$. The chains are held together mostly by electrostatic and steric interactions involving, respectively, the CF_3 and the CH_3 groups, which lie at the surface of such tubular chains [F \cdots F, $2.864(5)$ – $2.867(4) \text{ \AA}$]. Noteworthy is the presence of a

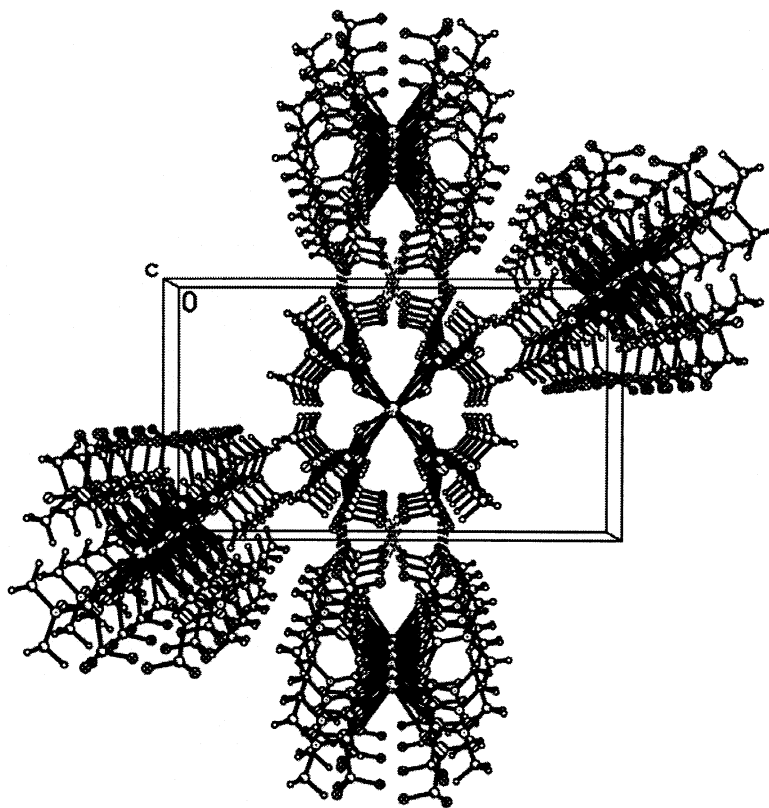


Figure 4. Crystal packing of the $\text{Sr}(\text{DMF})_2(\text{O}_3\text{SCF}_3)_2$ compound along the c axis.

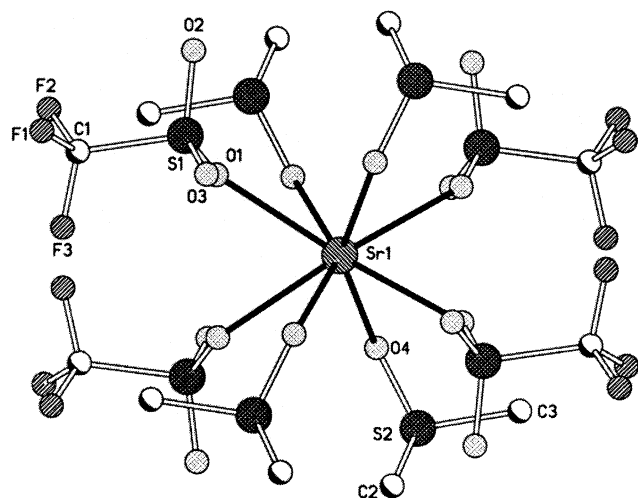


Figure 5. Ball-and-stick representation of the $\text{Sr}(\text{DMSO})_2(\text{O}_3\text{SCF}_3)_2$ coordination polyhedron.

weak *intramolecular* hydrogen bond $\text{C}-\text{H}\cdots\text{F}$ [$\text{C}2-\text{H}2$, 0.93(5) Å; $\text{H}2\cdots\text{F}2$, 2.53(5) Å; $\text{C}2\cdots\text{F}2$, 3.456(6) Å; $\text{C}2-\text{H}2\cdots\text{F}2$, 176(5)°]. Geometrical parameters dealing with the same structure collected at room temperature instead of low temperature show the following features: (1) larger gap between the $\text{Sr}-\text{O}$ bond lengths [$\text{Sr}1-\text{O}1$, 2.578(3) Å; $\text{Sr}1-\text{O}3$, 2.600(2) Å; average $\text{Sr}-\text{O}$, 2.589 Å]; (2) larger $\text{Sr}\cdots\text{Sr}$ distance [4.067(1) Å] due to the increase of the volume of the cell.

The structure of $\text{Sr}(\text{DMSO})_2(\text{O}_3\text{SCF}_3)_2$ (Figure 5) is similar to the one already discussed but shows less symmetry. It is made of one-dimensional chains along the *a* axis (Figure 6) with the metal cation lying on a binary axis. The coordination geometry around the Sr^{2+} ion is square antiprism showing some slight

deviation [α values ranging from 54.4° to 63.3°]. As for $\text{Sr}(\text{DMF})_2(\text{O}_3\text{SCF}_3)_2$, the $\text{Sr}-\text{O}$ bond distances are different for the two ligands [$\text{Sr}-\text{O}(\text{O}_3\text{SCF}_3)_{\text{av}}$, 2.587(8) Å and $\text{Sr}-\text{O}(\text{DMF})_{\text{av}}$, 2.649(8) Å], but the difference is greatly enhanced. However, the way that ligands bridge the Sr^{2+} ions is exactly the same as that observed in $\text{Sr}(\text{DMF})_2(\text{O}_3\text{SCF}_3)_2$. Within the polymeric chains, the $\text{Sr}\cdots\text{Sr}$ distance is 4.215(1) Å. The crystal packing shows steric and electrostatic interactions among the CH_3 and CF_3 groups [$\text{F}\cdots\text{F}$ distances vary from 2.80(1) to 2.84(1) Å], as well as weak *intra*- and *intermolecular* hydrogen bonds between the methyl groups and the CF_3SO_3^- O2 and O3 atoms.

The homologous Eu^{2+} compounds have not been reported in that study; all attempts to precipitate a Eu^{2+} DMF solvate lead to an oxidation characterized by a Eu^{3+} signal in the XANES spectrum. However, no detectable oxidation occurs for at least 3 h during the Eu^{2+} DMF solution measurement.

XAFS Analysis of the Eu^{2+} and Sr^{2+} Ions in DMF, DMSO, and MeCN Solutions. In a previous paper, we reported the XAFS study of the Eu^{2+} and Sr^{2+} ions first coordination sphere in aqueous solution. The Sr^{2+} ion was found to be octahydrated in aqueous solution, whereas the Eu^{2+} ion occurs as an equilibrium between a highly predominant $[\text{Eu}(\text{H}_2\text{O})_7]^{2+}$ ion and a minor $[\text{Eu}(\text{H}_2\text{O})_8]^{2+}$ species.¹

In aqueous solutions, it is well established that the triflate ion does not enter the first coordination sphere of solvated metal ions. In the nonaqueous DMF, DMSO, and MeCN solvents with smaller dielectric constants than water, it is important to ensure that no inner sphere ion pairing occurs between the metal and the triflate ions. Ion pair formation would strongly complicate the analysis of the XAFS data. Fortunately, the CF_3SO_3^- ion is a weak nucleophile, although there is some evidence that it is a slightly stronger coordinator than ClO_4^- in solution. However,

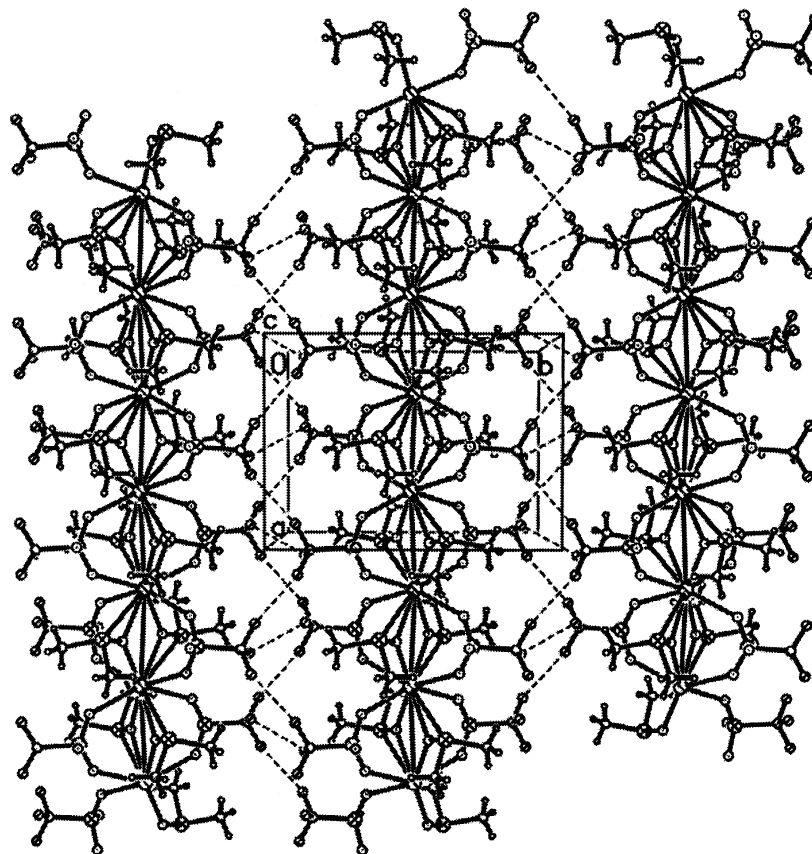


Figure 6. Crystal packing of the $\text{Sr}(\text{DMSO})_2(\text{O}_3\text{SCF}_3)_2$ compound along the *c* axis.

TABLE 3: First-Shell Structural Data Obtained from XAFS Analysis with Theoretical Phase and Amplitude at Room Temperature^a

cluster	<i>N</i>	<i>C</i> ₁ (Å)	<i>C</i> ₂ (Å ²)	<i>C</i> ₃ (Å ³) × 10 ⁻⁴	Δ <i>k</i>	ε × 10 ⁻²
Sr(DMF) ₂ (O ₃ SCF ₃) ₂ Powder						
SrO ₈ (H ₂ O) ₁₆ (OH) ₈	8.0	2.570	0.0107	1	1.5–11.5	1.7
Sr(DMF) ₄ (O ₃ SCF ₃) ₄	8.0	2.576	0.0108	2	1.5–11.5	0.8
Sr(DMSO) ₆	7.8	2.569	0.0102	2	1.5–11.5	2.0
Sr(DMSO) ₈	7.8	2.574	0.0104	3	1.5–11.5	1.6
Sr(DMSO) ₂ (O ₃ SCF ₃) ₂ Powder						
SrO ₈ (H ₂ O) ₁₆ (OH) ₈	7.5	2.590	0.0115	3	1.5–9.5	0.6
Sr(DMF) ₄ (O ₃ SCF ₃) ₄	7.9	2.592	0.0115	3	1.5–10	0.7
Sr(DMSO) ₆	7.5	2.580	0.0109	3	2–9.5	1.7
Sr(DMSO) ₈	7.7	2.588	0.0113	5	1.5–9.5	1.6
Sr(O ₃ SCF ₃) ₂ 0.15 M in DMF						
SrO ₈ (H ₂ O) ₁₆ (OH) ₈	7.0	2.535	0.0115	1	1.5–9	2.0
Sr(DMF) ₄ (O ₃ SCF ₃) ₄	6.9	2.544	0.0108	3	1.5–9	1.5
Sr(DMSO) ₆	6.8	2.546	0.0107	4	1.5–9	1.4
Sr(DMSO) ₈	6.7	2.546	0.0110	3	1.5–9	1.6
Sr(O ₃ SCF ₃) ₂ 0.15 M in DMSO						
SrO ₈ (H ₂ O) ₁₆ (OH) ₈	6.6	2.522	0.0100	0	1.5–11.5	1.1
Sr(DMF) ₄ (O ₃ SCF ₃) ₄	7.1	2.529	0.0105	1	1.5–11.5	0.8
Sr(DMSO) ₆	7.0	2.530	0.0103	2	2–10.5	0.9
Sr(DMSO) ₈	6.9	2.529	0.0103	1	1.5–11.5	0.8
Sr(O ₃ SCF ₃) ₂ 0.09 M in MeCN						
Sr(MeCN) ₆	8.1	2.649	0.0153	2.9	1.5–8	2.5
Sr(MeCN) ₈	8.2	2.652	0.0157	3.3	1.5–8	3.0
Eu(O ₃ SCF ₃) ₂ 0.15 M in DMF						
EuO ₈ (H ₂ O) ₁₆ (OH) ₈	5.8	2.531	0.0118	0	2.5–11.5	1.6
Eu(DMF) ₄ (O ₃ SCF ₃) ₄	6.2	2.531	0.0115	0	2.3–10	2
Eu(DMSO) ₆	6.1	2.529	0.0120	0	2.9–10.5	0.4
Eu(DMSO) ₈	5.8	2.527	0.0119	0	2.3–10	0.9
Eu(O ₃ SCF ₃) ₂ 0.10 M in MeCN						
Eu(MeCN) ₆	8.0	2.625	0.0174	2.5	2–10.5	0.3
Eu(MeCN) ₈	7.7	2.623	0.0170	2.7	1.7–11	0.3

^a *N* is the number of atoms located in the first shell, *C*₁ is the first cumulant, *C*₂ = *σ*² is the DW factor, *C*₃ is the third cumulant characterizing the asymmetry of the RDF, Δ*k* is the fitting interval, and ε is the fitting error.

CF₃SO₃⁻ is the best counterion for our purpose as ClO₄⁻ is potentially explosive in nonaqueous solutions or in the presence of a highly reducing agent such as Eu²⁺. The increasing solvation series MeCN < H₂O ~ DMF < DMSO²⁶ has been established for hard metal ions such as trivalent lanthanides. Therefore, the triflate ion will not enter the first coordination sphere in DMF and DMSO, which are better coordinating solvents than water. Note that the coordination of the triflate ion in the solid solvates Sr(DMF)₂(O₃SCF₃)₂ and Sr(DMSO)₂(O₃SCF₃)₂ may be explained by packing interactions in the crystals. Ion pairing is more likely to happen in the less-coordinating solvent MeCN. However, in this solvent, the presence of a triflate oxygen atom in the first shell of scatterers around the metal ion should lead to severe distortions into the XAFS spectra. Such distortions were not encountered during the XAFS analyses. Moreover, the very small amount of very poorly coordinating ethanol (EtOH) introduced during the preparation of the solutions does not compete with DMF and DMSO toward Eu²⁺ and Sr²⁺ coordination. It has been shown that despite the low coordination properties of the MeCN molecule, EtOH-free acetonitrile solvates were obtained by trans-solvation from alcoholic solvates.²⁷ As a consequence, interactions between metal and triflate ions or EtOH could be neglected in this study.

Table 3 summarizes the results from the analyses with theoretical phases and amplitudes and shows that no real improvement is attained by the use of one cluster over another.

TABLE 4: First-Shell Structural Data Obtained from XAFS Analysis with Theoretical Phase and Amplitude at Room Temperature, Synthetic Table^a

sample	<i>N</i>	<i>C</i> ₁ (Å)	<i>R</i> (Å)	<i>C</i> ₂ (Å ²)	<i>C</i> ₃ (Å ³) × 10 ⁻⁴
Sr(DMF) ₂ (O ₃ SCF ₃) ₂	7.9(3)	2.572(4)	2.582(4)	0.0106(4)	2(1)
Sr(DMSO) ₂ (O ₃ SCF ₃) ₂	7.8(3)	2.588(8)	2.598(8)	0.0112(8)	3(2)
Sr ²⁺ DMF solution	6.9(3)	2.545(5)	2.555(5)	0.0110(8)	3(2)
Sr ²⁺ DMSO solution	7.0(3)	2.530(7)	2.540(7)	0.0103(4)	1(1)
Sr ²⁺ MeCN solution	8.1(8)	2.651(6)	2.665(6)	0.0155(4)	3(1)
Eu ²⁺ DMF solution	6.0(5)	2.530(3)	2.541(3)	0.0118(8)	0.0(5)
Eu ²⁺ MeCN solution	7.9(4)	2.624(4)	2.640(4)	0.0172(4)	3(1)

^a *N* is the number of atoms located in the first shell at a distance *R* from the metal, *C*₁ is the first cumulant, *C*₂ = *σ*² is the DW factor, *C*₃ is the third cumulant characterizing the asymmetry of the RDF. These data have been arithmetically averaged from the fitting results presented in Table 3. Estimated errors are presented within parentheses.

Consequently, the values obtained with the different clusters have been arithmetically averaged and are presented in Table 4. The errors presented have been evaluated accounting for both systematical and statistical errors. Whereas the systematical errors were accounted for by a change of reference cluster, statistical errors (including correlations among parameters) were estimated by extensive fitting of the experimental first-shell XAFS spectra. Outside the fitting intervals indicated, the fitting errors were at least doubled.

In the high-energy XAFS region (EXAFS), the single scattering from the first shell of scatterers is dominant and can be analyzed quantitatively, as in the case of the Eu²⁺ and Sr²⁺ aqua ions.¹ In solvents such as DMSO, the contribution of the second shell of scatterers is not negligible and can be used to extract information about the configuration of the coordinated ligands.²⁸ Among these contributions, it has been shown that only the contributions of the M••S single scattering (SS) and of the M–O–S multiple scattering (MS) pathways are significant.^{18,29–31} The FT of the experimental XAFS spectrum of the Sr²⁺ ion in the DMSO solution (Figure 7) presents a first peak at 2.530(7) Å and a second peak at 3.73(2) Å corresponding to the DMSO sulfur atom (3.647(3) Å in the Sr(DMSO)₂(O₃SCF₃)₂ crystalline compound). Assuming a S–O bond distance of 1.529 Å in the coordinated DMSO,³² we obtained a mean Sr–O–S angle of 132(2)° in DMSO solution, typical for a hard acceptor,³² close to the one observed in the Sr(DMSO)₂(O₃SCF₃)₂ crystalline compound [133.6(2)°] and identical to the one observed for Y³⁺ in DMSO solution.²⁹ Note that the XAFS spectrum corresponding to the Eu²⁺ ion in DMSO solution has not been reported in this study because of the extreme absorption of the solvent in this energy region, preventing us from obtaining any XAFS signal in transmission mode.

The FT of the Eu²⁺ and Sr²⁺ experimental XAFS spectra in DMF solution consists in only one contribution at 2.530(3) and 2.545(5) Å, respectively (Figure 7), corresponding to the first shell of scatterers. In the liquid phase, no significant contribution from a second shell of scatterers or multiple scattering is observed in the XAFS FT, whereas the DMF carbonyl carbon atom should have a contribution. The carbon atom being a light scatterer, the intensity of the SS M••C contribution is small. It is additionally partly canceled by destructive interference with the MS M–O–C path, which is in antiphase. This, associated to a disordered first solvation sphere leading to a broad distribution of M••C distances, would make the carbon atom hardly detectable by XAFS. Therefore, taking into account only the first shell of scatterers is sufficient in first approximation to interpret the experimental XAFS spectra for both ions.

TABLE 5: Fit with Experimental Phase and Amplitude of Sr²⁺ and Eu²⁺^a

	<i>N</i>	<i>R</i> (Å)	<i>C</i> ₂ (Å ²)	<i>C</i> ₃ (Å ³) × 10 ⁻⁴	Δ <i>k</i>	ε × 10 ⁻²
Fit with Experimental Phase and Amplitude from the Solid Sr(DMF) ₂ (OTf) ₂						
Sr(DMF) ₂ (O ₃ SCF ₃) ₂	8.0 ^b	2.589 ^b	0.0106 ^c	2 ^c		
Sr(DMSO) ₂ (O ₃ SCF ₃) ₂	8.0(2)	2.603(2)	0.0116(2)	2(2)	1.5–10.5	0.6
Sr ²⁺ DMF solution	7.0(2)	2.556(3)	0.0110(5)	3(2)	1.5–9	1.4
Sr ²⁺ DMSO solution	7.0(2)	2.548(3)	0.0110(5)	0.5(5)	1.5–10.5	1.3
Fit with Experimental Phase and Amplitude from the Aqueous Sr ²⁺ Ion						
Sr ²⁺ aqua ion	8.0 ^d	2.600 ^d	0.0126 ^d	2.5 ^d		
Sr(DMF) ₂ (O ₃ SCF ₃) ₂	7.8(3)	2.596(4)	0.0112(5)	2(2)	1.5–11.5	2.1
Sr(DMSO) ₂ (O ₃ SCF ₃) ₂	7.6(4)	2.607(2)	0.0122(5)	2(2)	1.5–11.5	1.5
Sr ²⁺ DMF solution	6.9(4)	2.560(4)	0.0107(8)	3(2)	1.5–9	2.4
Sr ²⁺ DMSO solution	6.7(4)	2.552(3)	0.0115(5)	1(1)	1.5–9	2.7
Fit with Experimental Phase and Amplitude from the Aqueous Eu ²⁺ Ion						
Eu ²⁺ aqua ion	7.2 ^d	2.584 ^d	0.0138 ^d	1.5 ^d		
Eu ²⁺ DMF solution	6.1(5)	2.542(4)	0.0123(8)	0.5(5)	2–10	1.4

^a *N* is the number of atoms located in the first shell at a distance *R* from the metal, *C*₁ is the first cumulant, *C*₂ = *σ*² is the DW factor, *C*₃ is the third cumulant characterizing the asymmetry of the RDF, Δ*k* is the fitting interval, and ε is the fitting error. Estimated errors are presented within parentheses. ^b Crystallographic parameters. ^c Data from Table 4. ^d Data from ref 1.

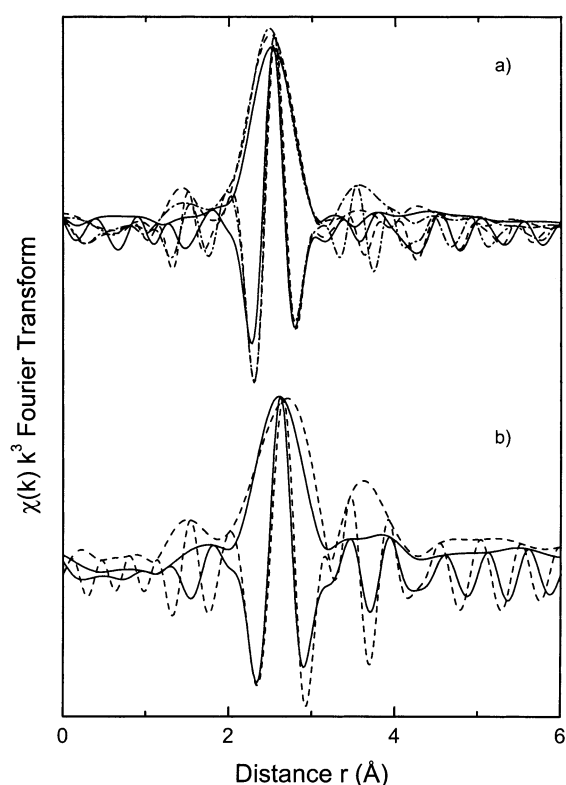


Figure 7. Comparison between Fourier transforms (modulus and imaginary parts) of the experimental XAFS, $\chi(k)k^3$, spectra of (a) 0.15 M Eu(O₃SCF₃)₂ in DMF (—), 0.15 M Sr(O₃SCF₃)₂ in DMF (---), and 0.15 M Sr(O₃SCF₃)₂ in DMSO (-·-) and (b) 0.10 M Eu(O₃SCF₃)₂ in MeCN (—) and 0.09 M Sr(O₃SCF₃)₂ in MeCN (---). These Fourier transforms have been corrected for the photoelectron phase shift using the theoretical phase and amplitude, and the Eu²⁺ solution imaginary part has been inverted for clarity.

The FT of the Sr²⁺ experimental XAFS spectrum in MeCN solution also features a first peak at 2.651(6) Å and a second around 3.8 Å (Figure 7). The relative intensities of these peaks match well the two principal shells of low-*Z* scatterers observed in the case of Cu(I) and Cu(II)³¹ and attributed, respectively, to Cu–N and Cu···C distances. Because of the MeCN linear geometry, the Sr²⁺ ion, the nitrogen, and the carbon atoms are almost collinear. Consequently, the SS and MS contributions of the nitrile group carbon atom are strongly enhanced because of a classical “focusing effect”, whereas they were negligible in the case of the DMF solution. The 3.78(3) Å Sr···C distance

found suggests that the Sr–N–C angle is quasi-linear in solution. The XAFS FT spectrum of the Eu²⁺ ion in MeCN solution features a first Eu–N peak at 2.624(4) Å (Figure 7). Moreover, a characteristic pattern in the imaginary part, very close to the one observed for the Sr²⁺ ion, shows that the double peak around 3.8 Å is not part of the noise but due to the presence of C atoms in a second scatterer shell. The 3.76(2) Å Eu···C distances found also suggests that the Eu–N–C angle is quasi-linear in solution.

Solutions in DMF and DMSO have also been analyzed using experimental phases and amplitudes extracted from the Sr(DMF)₂(O₃SCF₃)₂ crystalline reference and using the Eu²⁺ and Sr²⁺ aqua ions in solution¹ as an experimental reference. The obtained values (Table 5) are very close to the ones obtained with the theoretical approach (Table 4) with respect to the experimental errors. And because experimental phases and amplitudes are not available for the MeCN solutions, we decided for consistency sake to consider the values presented in Table 4 as the reference values through the rest of this paper.

In the study of the Eu²⁺ and Sr²⁺ aqua ions,¹ only one shell of scatterers was fitted. With a second shell of scatterers, the number of fitted parameters is doubled. Thus, the direct fitting of the unfiltered experimental spectra including two shells of scatterers leads to smaller fitting errors than those reported in Table 3. However, we observed in that case that the correlations among parameters were greatly enhanced. As a consequence, this fitting error decrease is thought to be only due to the increase in the number of adjustable parameters, and the two shells of scatterers were finally fitted separately. The XAFS experimental spectra after first-shell filtering are presented for Sr²⁺ and Eu²⁺ solutions in Figure 8, together with the fitted spectra with theoretical phases and amplitudes corresponding to the M(OSC₂)₆ and M(NCC)₈ clusters (Table 3). The low residual intensities (dotted lines) demonstrate the quality of these fits.

The radial distribution functions (RDF) for the first shell of scatterers of the Sr²⁺ and Eu²⁺ solutions were also simulated from the fitted parameters (Table 4) using the asymmetric approximation. They are compared in Figure 9. The *C*₃ cumulant measuring the skewing of distribution is rather low in all cases, showing the small asymmetric character of the RDF. The *C*₄ cumulant, which measures the weight in the tails of distribution, was fitted and found negligible in all solutions.

X-ray Absorption Edge Analysis. The low-energy part of the XAFS spectrum is known to contain information about the

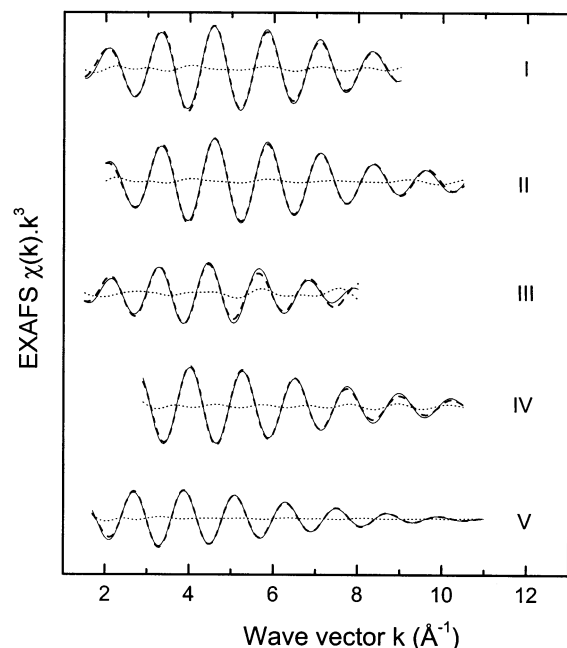


Figure 8. Experimental XAFS spectra of the Sr^{2+} ion in DMF (I), DMSO (II), and MeCN (III) and of the Eu^{2+} ion in DMF (IV) and MeCN (V) after first-shell filtering (—) compared with the fitted spectra with theoretical phases and amplitudes corresponding to the $\text{M}(\text{OSC}_2)_6$ and $\text{M}(\text{NCC})_8$ clusters (---). Residual curves are also represented (···), and fitting parameters are detailed in Table 3.

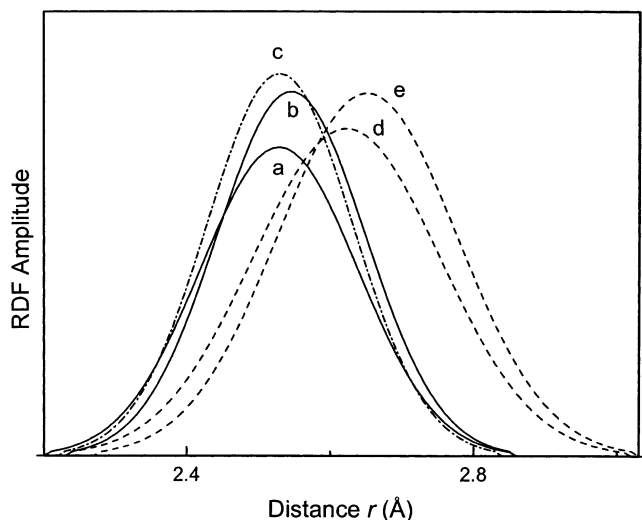


Figure 9. Reconstructed RDF of the first shell of scatterers using asymmetric approximations for (a) 0.15 M $\text{Eu}(\text{O}_3\text{SCF}_3)_2$ in DMF (—), (b) 0.15 M $\text{Sr}(\text{O}_3\text{SCF}_3)_2$ in DMF (---), (c) 0.15 M $\text{Sr}(\text{O}_3\text{SCF}_3)_2$ in DMSO (-·-·), (d) 0.10 M $\text{Eu}(\text{O}_3\text{SCF}_3)_2$ in MeCN (---), and (e) 0.09 M $\text{Sr}(\text{O}_3\text{SCF}_3)_2$ in MeCN (---).

valence and coordination polyhedron around the absorbing atom.³³ The local density of vacant electronic states in an absorbing atom determines the X-ray absorption edge region extending a few electronvolts below and above the edge. This region is therefore very sensitive to the valence state of the absorbing atom. The X-ray absorption near-edge structure (XANES) region extending from the edge up to about 50 eV above corresponds to the full multiple resonances of the excited photoelectron scattered by neighboring atoms.³³ It contains stereochemical information and is consequently characteristic of the symmetry and coordination polyhedron of the absorbing atom. In this paper, we will confine ourselves to an empirical approach of the XANES region based on earlier works.^{34,35}

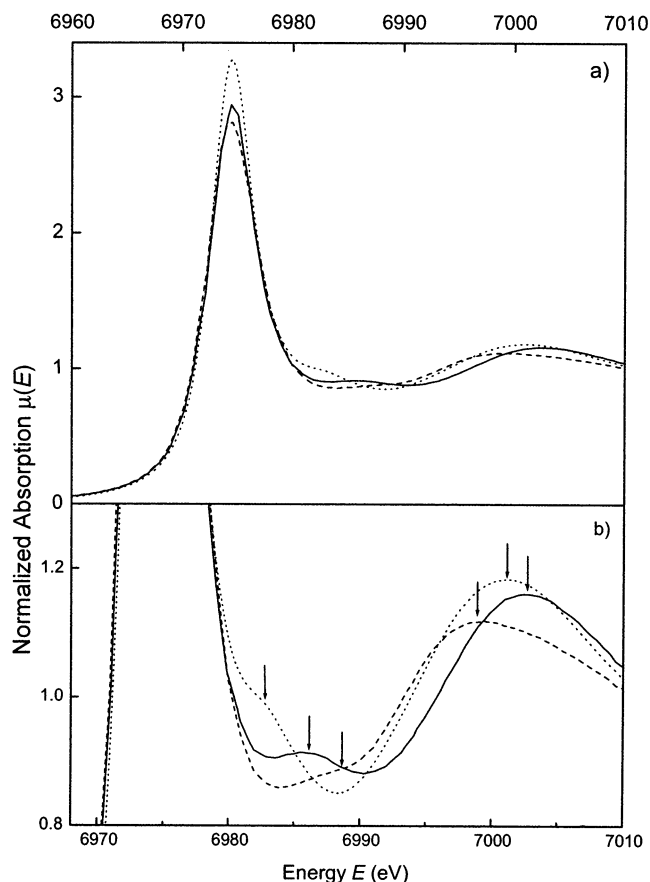


Figure 10. XANES Eu L_3 -edge spectrum (a) of $\text{Eu}(\text{O}_3\text{SCF}_3)_2$ 0.15 M in DMF (—), 0.10 M in MeCN (---), and 0.15 M in water (···) and (b) close-up on the structural XANES features.

Figure 10 presents the Eu L_3 -edge XANES spectra of the Eu^{2+} ion in DMF, MeCN, and H_2O . In all cases, the spectrum consists of a dominant white line (WL) resonance (normalized amplitude 2.8–3.2 at 6974 eV) corresponding to the transition from the $2p_{3/2}$ level to the unoccupied 5d states, followed by important multiple scattering contributions (first and second series of arrows). It has been shown in aqueous solution that amounts of Eu^{3+} smaller than 1% could be detected by XANES,¹ the Eu^{2+} and Eu^{3+} valence states being easily distinguished because of the different threshold energies of their WL. Eu L_3 -edge recorded spectra in DMF and MeCN (Figure 10) show no Eu^{3+} peak. Further XANES measurements also showed that no oxidation of the Eu^{2+} occurred after 2 h of measurement.

Contrary to the Eu^{2+} L_3 -edge spectra, no WL is present in the Sr K-edge XANES spectra of the Sr^{2+} ion in DMF, DMSO, MeCN, and H_2O (Figure 11). The Sr K-edges correspond to a transition from the 1s core level to the quasi-bound 4p and np orbitals (according to the dipole selection rules) that are involved in the metal-to-solvent bond. It is consequently very sensitive to changes in bond strength or in the coordination polyhedron. An increase in the edge energy is observed for the Sr^{2+} ion along the $\text{MeCN} < \text{H}_2\text{O} \ll \text{DMF} < \text{DMSO}$ series, as well as an increase of the first peak energy (first series of arrows in Figure 11). These features are well explained by the corresponding decrease of the metal-to-solvent bond length (Table 4), which is associated with a shift of the first peak toward higher energies. It can also be noted that the energy and the area of the first peak are very closed for the aqueous and MeCN solutions, on one hand, and for the DMF and DMSO solutions, on the other hand, indicating similarities in coordination numbers

TABLE 6: XAFS Structural Data for Sr²⁺ and Eu²⁺ Ions in Aqueous and Nonaqueous Solution, Comparison with Literature^a

sample	<i>N</i>	<i>R</i> (Å)	<i>C</i> ₂ (Å ²)	<i>C</i> ₃ (Å ³) × 10 ⁻⁴	ref
0.14 M Sr(O ₃ SCF ₃) ₂ in H ₂ O	8.0(3)	2.600(3)	0.0126(5)	2.7(5)	1
0.8 M Sr(ClO ₄) ₂ in H ₂ O	8 ^b	2.61(1)	0.0116(5)		18
0.1 and 3 M SrCl ₂ in H ₂ O	10.3(1)	2.643(2)	0.021(2)	β ^c	24
0.15 M Sr(O ₃ SCF ₃) ₂ in DMF	6.9(3)	2.555(5)	0.0110(8)	3(2)	this work
0.15 M Sr(O ₃ SCF ₃) ₂ in DMSO	7.0(3)	2.540(7)	0.0103(4)	1(1)	this work
1.30 M Sr(O ₃ SCF ₃) ₂ in DMSO	6 ^b	2.54(1)	0.0082(4)		18
0.09 M Sr(O ₃ SCF ₃) ₂ in MeCN	8.1(8)	2.665(6)	0.0155(4)	3(1)	this work
0.06 M Sr(O ₃ SCF ₃) ₂ in MeCN	8.0(2)	2.710(3)	0.024(1)	β ^c	36
0.15 M Eu(O ₃ SCF ₃) ₂ in H ₂ O	7.2(3)	2.584(5)	0.0138(5)	1.5(5)	1
0.15 M Eu(O ₃ SCF ₃) ₂ in DMF	6.0(5)	2.541(3)	0.0118(8)	0.0(5)	this work
0.10 M Eu(O ₃ SCF ₃) ₂ in MeCN	7.9(4)	2.640(4)	0.0172(4)	3(1)	this work

^a *N* is the number of atoms located in the first shell at a distance *R* from the metal, *C*₂ = *σ*² is the DW factor, *C*₃ is the third cumulant characterizing the asymmetry of the RDF, and total errors are presented within parentheses. ^b Parameter fixed. ^c Parameter related to the RDF asymmetry.

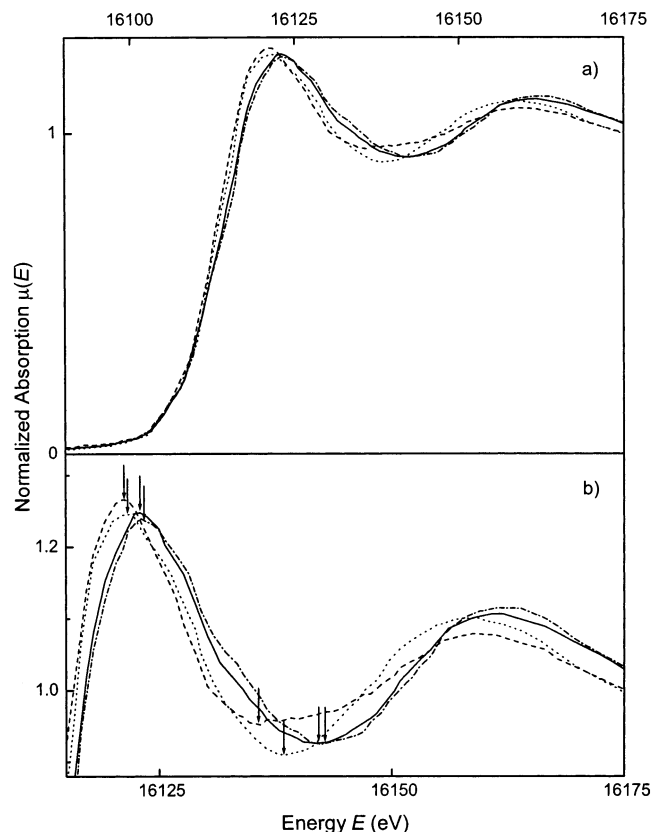


Figure 11. XANES Sr K-edge spectrum (a) of Sr(O₃SCF₃)₂ 0.15 M in DMF (—), 0.15 M in DMSO (---), 0.09 M in MeCN (- · -), and 0.14 M in water (···) and (b) close-up on the structural XANES features.

and in coordination structure. According to observation performed on plutonium aqua ions (oxidation states ranging from +III to +VI),³⁵ the decrease in symmetry associated with the decrease of coordination number from 8 to 7 could explain the broadening of the first peak observed between these two couples of solvents.

The first part of the Eu L₃-edge XANES spectra of the Eu²⁺ ion in DMF, MeCN, and H₂O (first series of arrows in Figure 10) cannot be interpreted without proper calculation. However, the important changes in their general shape tend to show that the coordination structure of the Eu²⁺ ion in H₂O, DMF, and MeCN solutions is different. Note that for both Eu²⁺ and Sr²⁺ XANES spectra, the first EXAFS oscillation (second series of arrows in Figures 10 and 11) is very similar even if inverted because of phase inversion between K- and L-edges. For both cations, the oscillation corresponding to the MeCN solution occurs first, then the oscillation for water, and finally that for

DMF and DMSO, according to the respective metal-to-solvent bond length.

Discussion

We recently studied the solvation of the Eu²⁺ and Sr²⁺ ions in water¹ and now report their solvation in DMF, DMSO, and MeCN. In the literature, only two references relevant to our study were found. Both of them were XAFS studies, one about Sr²⁺ solvation in DMSO¹⁸ and the other about Sr²⁺ solvation in MeCN.³⁶ Results for the Sr²⁺ aqua ion by the same authors^{18,24} are also reported in Table 6 for comparison.

Persson et al.¹⁸ performed LAXS and XAFS measurements on the solvated Sr²⁺ ion in DMSO. The radial distribution function (RDF) obtained by LAXS showed two peaks at 2.54(1) and 3.77(1) Å, leading to an average Sr–O–S angle of 136°. Because of the strong correlation between the fitting parameters, the authors resolved to test the following *N* values: 4, 5, 6, 8, and 10. The lowest error square sum was obtained with *N* = 6. In the LAXS measurements, high absorption of the DMSO solvent made it necessary to use short path lengths and high solute concentration (1.3 M in Sr(O₃SCF₃)₂ compared to the 11.3 M of pure DMSO). Not accounting for the MET effects, the authors could not fit the coordination number in the XAFS analysis. The *N* value was therefore fixed to 6, leading to a DW factor of 0.0082(4) Å² and a Sr–O bond length of 2.54(1) Å. Our MET-corrected XAFS analysis in diluted Sr²⁺ DMSO solution led to an *N* value of 7.0(3). Using *N* = 7 and taking into account a linear correlation between *N* and the DW factor, we can calculate a DW factor of 0.0096 Å² from Persson's data. This value is very close to the 0.0103(4) Å² value reported here. Besides the MET correction, the difference in coordination number could also be interpreted as a concentration effect. The Sr–O distances that we found are very close to those obtained by Persson et al. in both aqueous and DMSO solutions (Table 6).

D'Angelo et al.³⁶ performed an XAFS analysis on a 0.06 M Sr(O₃SCF₃)₂ in MeCN solution. They fitted the XAFS raw data (without FT) using a cluster based on a classical molecular dynamics simulation. They obtained a coordination number of 8.0(2) associated with a Sr–N distance of 2.710(3) Å and a DW factor of 0.024(1) Å². Our results are very similar even if the absolute values are different. We measured a metal-to-solvent distance increase of 0.065 Å and DW factor increase of 0.0029 Å² when going from water to the dry MeCN solution, compared to the reported values of 0.067 and 0.003 Å². We found a Sr···C contribution at 3.78(3) Å (they report 3.76(2) Å) and found an almost linear Sr–N–C angle, whereas they reported 149°.

Alkaline-earth metal ions and trivalent lanthanides are strongly solvated by hard donor solvents such as DMF (DN =

26.6) and DMSO (DN = 29.8) and weakly solvated by soft donor solvents such as MeCN (DN = 14.1). H_2O is intermediate with a donor number (DN) value of 18.0.³⁷ Actually, the decrease of the structural parameters (metal-to-solvent distance, coordination number, and DW factor) is correlated with increasing DN along the MeCN < H_2O < DMF < DMSO series for both the Eu^{2+} and Sr^{2+} cations (Table 6).

Our results show a one-unit decrease in coordination number when going from H_2O to DMF and DMSO solutions for both Eu^{2+} and Sr^{2+} ions. Such a decrease is expected, because DMF and DMSO are at the same time bulkier solvents and much better coordinators than H_2O . A decrease in coordination number from 7 for Sr^{2+} to 6 for Eu^{2+} is also observed in DMF. This decrease is not surprising, because it has already been observed from 8 to 7 in the aqueous solution.¹ In the MeCN solution, the same N value of 8 was found for both Eu^{2+} and Sr^{2+} ions. This suggests that in the case of the MeCN solution, the coordination number is mostly dependent on the electrostatic interactions and not on the steric hindrance. A tendency toward coordination number decrease is also observed between aqueous and DMF solutions for trivalent lanthanide ions.^{30,38} In the solid state, trivalent lanthanides are preferentially coordinated to 9 MeCN,^{22,39} to 9 H_2O ,^{40,41} to 8 DMF,⁴² and to 8 or 7 DMSO ligands,⁴³ depending of the size of the lanthanide cation. Hence, a decrease in coordination number is observed in the solid state of trivalent lanthanide solvates when increasing the solvation strength of the solvent along the series MeCN < H_2O < DMF < DMSO.³⁷ Such an effect is consequently not specific to the Eu^{2+} and the Sr^{2+} ions in solution but could be observed for other typical hard ions. Note that a steric hindrance effect on coordination number has also been observed among trivalent lanthanides in the very similar DMF and DMA (*N,N*-dimethyl acetamide) solvents (respective DN values of 26.6 and 27.8).³⁷ The decrease in coordination number occurring from DMF to DMA³⁸ shows that hard ions are subjected to strong solvation steric effects in bulky aprotic oxygen-donor solvents.

For both Eu^{2+} and Sr^{2+} ions, the metal-to-solvent distances decrease along the MeCN > H_2O > DMF \approx DMSO series (Table 6). Moreover, in all of the solvents considered, these distances are slightly shorter for Eu^{2+} than for the Sr^{2+} ion (without coordination number correction). In the MeCN solutions, a 0.025 Å decrease is observed (larger than the 0.01 Å decrease derived from Shannon radii⁴⁴ for $N = 8$). In the O-coordinating solvents, a 0.014–0.016 Å decrease is observed, whereas the associated coordination number decrease should lead to more severe shortening of the bond lengths (0.04–0.06 Å according to Shannon⁴⁴). The Eu^{2+} ion seems to have a slightly higher affinity toward MeCN and a slightly lower affinity toward O-coordinating solvents when compared with the Sr^{2+} ion. Actually, we observe in the X-ray diffraction (XRD) structures of the Eu^{2+} and Sr^{2+} diethylenetriamine pentaacetic acid (DTPA) complexes,⁴⁵ on average, 0.013 Å shorter M–N bond lengths and 0.011 Å longer M–O bond lengths for the Eu^{2+} over the Sr^{2+} ion. In isomorphous acetates,^{46,47} the Eu–O bond lengths were 0.015 Å longer than their Sr^{2+} homologues. Hence, the comparison of crystallographic data of the solid state, as well as the comparison of metal-to-solvent bond length in solution, suggests that the Eu^{2+} and Sr^{2+} ionic radii are equivalent and that Eu^{2+} is a slightly softer ion than Sr^{2+} , leading to shorter M–N bonds and longer M–O bonds. Eu^{2+} being the same size as Sr^{2+} , its relative softness could be due to the presence of 25 extra electrons. The difference in hardness could therefore explain the rather small bond length decrease observed in the O-coordinating solvents,

because it partly compensates the decrease associated in the coordination number diminution. A higher polarizability would also explain the tendency toward lower coordination numbers observed for the Eu^{2+} ion in O-donor solvents.

The Debye–Waller (DW) factor can be related to the width of the radial distribution function (RDF); as the DW factor becomes larger, the distribution of the bond lengths becomes larger. An increase of the DW factor could therefore either correspond to a low symmetry polyhedron or to an equilibrium between species with different coordination numbers (i.e., different metal-to-solvent bond lengths). In solution, the DW factor increases significantly from the highly coordinating DMF and DMSO to the small H_2O , and then to the low-coordinating MeCN. In the same solvent, the Eu^{2+} DW factor is 7%–10% larger than that of the Sr^{2+} ion. The coordination numbers and low DW values found in DMF and DMSO solutions suggest that the $[\text{Sr}(\text{DMF})_7]^{2+}$, $[\text{Eu}(\text{DMF})_6]^{2+}$, and $[\text{Sr}(\text{DMSO})_7]^{2+}$ ions are the only solvates present in solution. The coordination numbers found in MeCN solutions suggest that the octa-coordinated ions $[\text{Sr}(\text{MeCN})_8]^{2+}$ and $[\text{Eu}(\text{MeCN})_8]^{2+}$ are the predominant species in solution, but the associated high DW values do not exclude an equilibrium with minor 7 or 9 coordinated solvates or both.

To the best of our knowledge, the same coordination number was found in pure DMF and in pure DMSO, whatever the metal ion.^{48,49} Therefore, the 6 coordination number found for the $[\text{Eu}(\text{DMF})_6]^{2+}$ ion would suggest hexa-coordination for the Eu^{2+} ion in DMSO solution, for which no experimental data are available. From the structural parameters found for the Sr^{2+} ion in the MeCN, H_2O , DMF, and DMSO solutions and from the comparison between Eu^{2+} and Sr^{2+} ions in these different solvents, we can deduce for the $[\text{Eu}(\text{DMSO})_6]^{2+}$ ion a Eu–O bond length of 2.525 Å and a DW factor close to 0.0112 Å².

Conclusion

Structural parameters of the Eu^{2+} ion were established in DMF and MeCN solutions, as well as the structural parameters for Sr^{2+} in DMF, DMSO, and MeCN solutions, using the XAFS method with picometer accuracy. We obtained for the Eu^{2+} ion in DMF and MeCN solutions coordination numbers of 6.0(5) and 7.9(4) and metal-to-solvent distances of 2.541(3) and 2.640(4) Å, respectively. A coordination number of 6 and a metal-to-solvent distance of 2.525 Å were extrapolated for the Eu^{2+} ion in DMSO solution, for which no experimental data are available. We obtained for the Sr^{2+} ion in DMF, DMSO, and MeCN solutions coordination numbers of 6.9(3), 7.0(3), and 8.1(8) and metal-to-solvent distances of 2.555(5), 2.540(7), and 2.665(6) Å, respectively.

For both Eu^{2+} and Sr^{2+} ions, a decrease in coordination number and metal-to-solvent distances was found along the increasingly solvating MeCN < H_2O < DMF < DMSO solvent series: for europium(II), $N = 8$ with $[\text{Eu}(\text{MeCN})_8]^{2+}$, $N = 7$ with $[\text{Eu}(\text{H}_2\text{O})_7]^{2+}$, and $N = 6$ with $[\text{Eu}(\text{DMF})_6]^{2+}$ and by extrapolation $[\text{Eu}(\text{DMSO})_6]^{2+}$; for strontium, $N = 8$ with $[\text{Sr}(\text{MeCN})_8]^{2+}$ and $[\text{Sr}(\text{H}_2\text{O})_8]^{2+}$ and $N = 7$ with $[\text{Sr}(\text{DMF})_7]^{2+}$ and $[\text{Sr}(\text{DMSO})_7]^{2+}$. However, an equilibrium with a minor amount of 7 or 9 coordinated solvates or both cannot be excluded in MeCN solution.

As is the case for the trivalent lanthanides,³⁸ Eu^{2+} and Sr^{2+} feature a strong solvation steric effect in solution when moving from water to bulky aprotic donor solvents, whereas in the MeCN solution, the interaction is mostly electrostatic and not very dependent on the steric hindrance effects. We also showed that Eu^{2+} and Sr^{2+} ionic radii should be considered as equivalent

and that Eu^{2+} seems to be a slightly softer ion than Sr^{2+} , leading to shorter M–N and longer M–O bonds and to smaller coordination numbers in O-coordinating solvents.

Acknowledgment. We thank F. Bouamrane, the LURE D21 beam line staff (R. Cortes, S. Bénazeth, I. Ascone) for their technical collaboration, and A. Kuzmin for his comments. We also thank the “Laboratoire pour l’Utilisation du Rayonnement Electromagnétique” (LURE) for the beam time allocation and laboratory facilities. We finally acknowledge the Swiss National Science Foundation, the Latvian National Science Foundation, and the COST actions D9 (Advanced Computational Chemistry of Increasingly Complex Systems) and D18 (Lanthanide Chemistry for Diagnosis and Therapy) for financial support.

Supporting Information Available: Crystallographic data in CIF format for the $\text{Sr}(\text{DMF})_2(\text{O}_3\text{SCF}_3)_2$ (143 and 293 K) and the $\text{Sr}(\text{DMSO})_2(\text{O}_3\text{SCF}_3)_2$ (143 K) compounds.

References and Notes

- Moreau, G.; Helm, L.; Purans, J.; Merbach, A. E. *J. Phys. Chem. A* **2002**, *106*, 3034.
- IUPAC Recommended Methods for Purification of Solvents and Tests for Impurities*; Coetzee, J. F., Ed.; Pergamon Press: Elmsford, NY, 1982.
- Mikheev, N. B.; Kamenskaya, A. N. *Coord. Chem. Rev.* **1991**, *109*, 1.
- Bunker, G. *Nucl. Instrum. Methods* **1983**, *207*, 437.
- Sayers, D. E.; Bunker, B. A. In *X-ray Absorption*; Koningsberger, D. C., Prins, R., Eds.; Chemical Analysis, Vol. 92; Wiley & Sons: New York, 1988.
- Crozier, E. D.; Rehr, J. J.; Ingalls, R. In *X-ray Absorption*; Koningsberger, D. C., Prins, R., Eds.; Chemical Analysis, Vol. 92; Wiley & Sons: New York, 1988.
- Rehr, J. J.; Mustre de Leon, J.; Zabinsky, S. I.; Albers, R. C. *J. Am. Chem. Soc.* **1991**, *113*, 5135.
- Dalba, G.; Fornasini, P.; Grisenti, R.; Purans, J. *Phys. Rev. Lett.* **1999**, *82*, 4240.
- Cooley, R. A.; Yost, D. M. *Inorg. Synth.* **1946**, *II*, 69.
- CrysAlis RED*, release 1.6.9 β ; Oxford Diffraction Ltd.: Abingdon, Oxfordshire, U.K., 2001.
- Blessing, R. H. *Acta Crystallogr., Sect. A* **1995**, *51*, 33.
- Walker, N.; Stuart, D. *Acta Crystallogr., Sect. A* **1983**, *39*, 158.
- Altomare, A.; Burla, M. C.; Camalli, M.; Cascarano, G. L.; Giacovazzo, C.; Guagliardi, A.; Moliterni, A. G. G.; Polidori, G.; Spagna, R. *J. Appl. Crystallogr.* **1999**, *32*, 115.
- SHELXTL*, release 5.1; Bruker AXS, Inc.: Madison, WI, 53719, 1997.
- Villain, F.; Briois, V.; Castro, I.; Helary, C.; Verdager, M. *Anal. Chem.* **1993**, *65*, 2545.
- Kuzmin, A. *Physica B* **1995**, *208–209*, 175.
- Dalba, G.; Fornasini, P. *J. Synchrotron Radiat.* **1997**, *4*, 243.
- Persson, I.; Sandstrom, M.; Yokoyama, H.; Chaudhry, M. Z. *Naturforsch.* **1995**, *50a*, 21.
- Nieuwenhuizen, M.; Wen, H.; Wilkins, C. J. *Z. Anorg. Allg. Chem.* **1992**, *615*, 143.
- Klinga, M.; Cuesta, R.; Moreno, J. M.; Dominguez-Vera, J. M.; Colacio, E.; Kivekas, R. *Acta Crystallogr., Sect. C* **1998**, *54*, 1275.
- Muller, U.; Noll, A. *Z. Kristallogr.* **2000**, *215*, 191.
- Deacon, G. B.; Görtler, B.; Junk, P. C.; Lork, E.; Mews, R.; Petersen, J.; Zemva, B. *J. Chem. Soc., Dalton Trans.* **1998**, 3887.
- Bunker, B. A.; Stern, E. A. *Phys. Rev. B* **1983**, *27*, 1017.
- D’Angelo, P.; Nolting, H.-F.; Pavel, N. V. *Phys. Rev. A* **1996**, *53*, 798.
- Kepert, D. L. In *Aspects of the stereochemistry of 8-coordination*; Lippard, S. J., Ed.; Progress in Inorganic Chemistry, Vol. 24; Wiley: New York, 1978; p 179.
- Bunzli, J.-C. G.; Milicic-Tang, A.; Gschneidner, K. A. J.; Eyring, L., Eds. *Handbook on the Physics and Chemistry of Rare Earths*; Elsevier Science B. V.: Amsterdam, 1995; Vol. 21.
- Gnaegi, F. Diploma Work, University of Lausanne, Lausanne, Switzerland, 1967.
- Teo, B. K. In *EXAFS and Near Edge Structure*; Bianconi, A., Incoccia, L., Stipcich, S., Eds.; Springer: Berlin, 1983; p 11.
- Lindqvist-Reis, P.; Naslund, J.; Persson, I.; Sandstrom, M. *J. Chem. Soc., Dalton Trans.* **2000**, 2703.
- Naslund, J.; Lindqvist-Reis, P.; Persson, I.; Sandstrom, M. *Inorg. Chem.* **2000**, *39*, 4006.
- Persson, I.; Penner-Hahn, J. E.; Hodgson, K. O. *Inorg. Chem.* **1993**, *32*, 2497.
- Calligaris, M.; Carugo, O. *Coord. Chem. Rev.* **1996**, *153*, 83.
- Bianconi, A. In *EXAFS and Near Edge Structure*; Bianconi, A., Incoccia, L., Stipcich, S., Eds.; Springer: Berlin, 1983; p 118.
- Purans, J.; Kuzmin, A.; Parent, P.; Laffon, C. *Electrochim. Acta* **2001**, *46*, 1973.
- Ankudinov, A. L.; Conradson, S. D.; Mustre de Leon, J.; Rehr, J. *J. Phys. Rev. B* **1998**, *57*, 7518.
- D’Angelo, P.; Pavel, N. V. *J. Chem. Phys.* **1999**, *111*, 5107.
- Gutmann, V. *The Donor–Acceptor Approach to Molecular Interactions*; Plenum Press: New York, 1978.
- Ishiguro, S.; Umabayashi, Y.; Komiya, M. *Coord. Chem. Rev.* **2002**, *226*, 103.
- Shen, Q.; Hu, J.-Y.; Jin, Z.-S.; Sun, Y. *J. Chin. Rare Earth Soc.* **1990**, *8*, 359.
- Gerkin, R. E.; Reppart, W. J. *Acta Crystallogr., Sect. C* **1984**, *C40*, 781.
- Harrowfield, J. M.; Kepert, D. L.; Patrick, J. M.; White, A. H. *Aust. J. Chem.* **1983**, *36*, 483.
- Krishnamurthy, S. S.; Soundararajan, S. *Can. J. Chem.* **1969**, *47*, 995.
- Krishnamurthy, V. N.; Soundararajan, S. *J. Inorg. Nucl. Chem.* **1967**, *29*, 517.
- Shannon, R. D. *Acta Crystallogr.* **1976**, *A32*, 751.
- Burai, L.; Toth, E.; Seibig, S.; Scopelliti, R.; Merbach, A. E. *Chem.–Eur. J.* **2000**, *6*, 3761.
- Starynowicz, P. *Polyhedron* **1995**, *14*, 3573.
- Trunov, V. K.; Chubinizde, A. D.; Efremov, V. A.; Velikodni, Y. A. *Koord. Khim.* **1984**, *10*, 403.
- Lincoln, S. F.; Merbach, A. E. In *Substitution reactions of solvated metal ions*; Sykes, A. G., Ed.; Advances in Inorganic Chemistry, Vol. 42; Academic Press: San Diego, CA, 1995; p 1.
- Ohtaki, H. *Monatsh. Chem.* **2001**, *132*, 1237.